

---

# CELL SEGMENTATION AND TRACKING USING DISTANCE TRANSFORM PREDICTIONS AND MOVEMENT ESTIMATION WITH GRAPH-BASED MATCHING

---

A PREPRINT

**Tim Scherr**

Institute for Automation and Applied Informatics  
Karlsruhe Institute of Technology (KIT)  
Karlsruhe, Germany  
tim.scherr@kit.edu

**Katharina Löffler**

Institute for Automation and Applied Informatics  
Karlsruhe Institute of Technology (KIT)  
Karlsruhe, Germany  
katharina.loeffler@kit.edu

**Moritz Böhlend**

Institute for Automation and Applied Informatics  
Karlsruhe Institute of Technology (KIT)  
Karlsruhe, Germany  
moritz.boehland@kit.edu

**Ralf Mikut**

Institute for Automation and Applied Informatics  
Karlsruhe Institute of Technology (KIT)  
Karlsruhe, Germany  
ralf.mikut@kit.edu

June 22, 2021

## ABSTRACT

In this paper, we present the approach used for our IEEE ISBI 2020 Cell Tracking Challenge<sup>1</sup> contribution (team KIT-Sch-GE). Our method consists of a segmentation and a tracking step that includes the correction of segmentation errors (tracking by detection method). For the segmentation, deep learning-based predictions of cell distance maps and novel neighbor distance maps are used as input for a watershed post-processing. Since most of the provided Cell Tracking Challenge ground truth data are 2D, a 2D convolutional neural network is trained to predict the distance maps. The tracking is based on a movement estimation in combination with a matching formulated as a maximum flow minimum cost problem.

## 1 Introduction

State-of-the-art microscopy imaging techniques such as fluorescence microscopy imaging enable, for instance, to investigate cell dynamics with single-cell resolution [1]. This allows to study cell migration and proliferation in tissue development. Therefore, it is necessary to segment and track individual objects virtually error-free over time, e.g., to establish the required complete lineage of each cell within an organism [1, 2]. Due to the large amount of data acquired with modern imaging techniques, manual data analysis is impossible. Additionally, low-resolution objects are very difficult to detect even for human experts. Deep learning-based segmentation methods have proven to outperform classical methods even on very diverse 2D data sets [3]. However, state-of-the-art tracking methods often still need some time-consuming manual cell track curation, e.g., using EmbryoMiner [4], especially for low signal-to-noise ratio and 3D data [5].

Classical segmentation methods, such as TWANG [6] for the segmentation of roundish objects, often need to be adapted to the cell type and to the imaging conditions used. Therefore, expert knowledge is needed. In contrast, deep learning-based segmentation methods shift the expert knowledge needed to the training process. Thus, less expert knowledge is needed for the application of a trained model and to fine-tune the post-processing which is often kept

---

<sup>1</sup><http://celltrackingchallenge.net/>

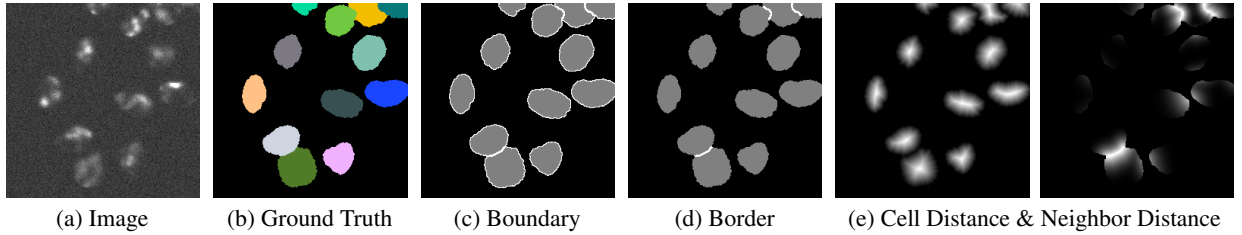


Figure 1: Training data representations for the training of deep learning models. Boundaries (c) and borders (d) can be used to split touching cell nuclei. Many training data sets contain only few touching nuclei resulting in few training samples for borders and boundaries in between nuclei. The neighbor distance labels (e) are aimed to solve this problem since models can also learn from non-touching nuclei. The image (a) shows a crop from the simulated data set Fluo-N2DH-SIM+ of the Cell Tracking Challenge [5, 22].

very simple. To improve the generalization ability of a trained deep learning model, a diverse annotated data set is needed. In addition, an appropriate training data representation may help. For the segmentation of touching cell nuclei, deep learning models can be trained to predict boundaries or borders (see Figure 1), e.g., in [7]. However, predicted boundaries may not be closed especially in between touching cells and predicted borders may not be robust enough which both results in the merging of cells [7, 8]. Training models to predict adapted thicker borders and smaller cells can decrease the amount of merged cell nuclei [8, 9]. A lot of effort is put into finding better representations to improve the segmentation of touching nuclei. Li et al. combine distance transforms for single cell nuclei and discrete boundaries [10]. Li, Hu and Yang propose a center vector encoding which should also be more robust to label inconsistencies [11]. Graham et al. use horizontal and vertical gradient maps [12].

Although deep learning has been successfully applied to multi object tracking on natural images [13, 14], there are only few deep learning approaches for cell tracking [15, 16]. Payer et al. simultaneously segment and track cells by combining a recurrent hourglass network with a pixel-wise metric embedding learning [15]. He et al. propose a particle filter based motion model in combination with a CNN-based observation model [16]. However, cell tracking is still dominated by classical tracking approaches [5, 17]. A possible reason is the lack of high quality annotations as provided in natural image tracking benchmarks [18, 19, 20] and therefore the missing training data. Another aspect aggravating the task of cell tracking are cell death and division events, which do not occur in natural image tracking data. Therefore, classical tracking algorithms with comparably few parameters and explicit modeling of cell division events still dominate cell tracking benchmarks [5]. The comparison of cell tracking algorithms by Ulman et al. shows a majority of tracking approaches use an adapted version of nearest neighbors, a graph-based linking or multi hypothesis tracking [5]. Furthermore, Magnusson et al. apply the Viterbi algorithm to cell tracking [17], whereas Sixta et al. model object tracking as Bayes risk minimization [21].

In this paper, we describe our IEEE ISBI 2020 Cell Tracking Challenge contribution (team KIT-Sch-GE) and propose a novel training data representation, the neighbor distances, to solve the challenging problem of segmenting touching cell nuclei. The neighbor distances are aimed to be more robust to annotation inconsistencies resulting in a better generalization ability of the trained deep neural network. For tracking, we adapt a minimum cost flow algorithm to include object movement estimation and re-link tracks with missing segmentation masks.

## 2 Methods

### 2.1 Segmentation

**Training Data Representation** A key for the successful application of supervised deep learning methods in the absence of large training data sets is to learn representations which generalize well. Therefore, instead of the often used cell and cell border representations (to get markers for a marker-based watershed post-processing), we combine cell distance transforms [10] and a novel form of neighbor distance transforms. Figure 1 shows exemplary distance transform labels using Euclidean distance transforms. The transforms of each single cell and of the neighbors are normalized to the range  $[0, 1]$ . The neighbor distances are closed using grayscale closing and taken to the power of 3 to get a steeper decline within cells. In principle, this cell distance is sufficient to get markers for the post-processing if a model is well trained. However, the neighbor distances are aimed to reduce the probability to merge cells. Figure 2 shows that the distance transform representations are more robust to annotation inconsistencies than boundaries and

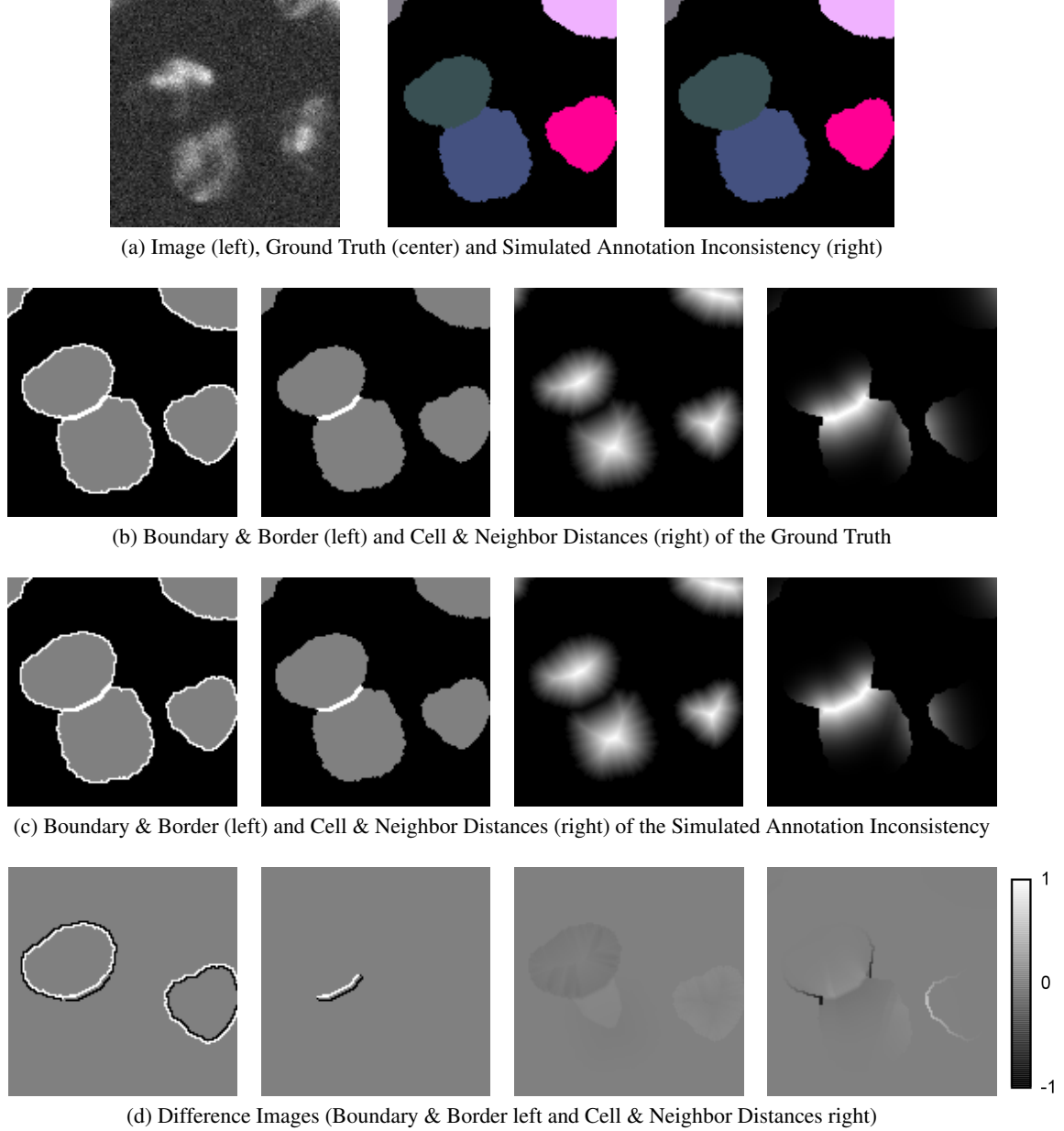


Figure 2: Robustness to annotation inconsistencies. Small changes in the ground truth (a) result in different boundaries and borders (b and c). The difference images (d) between (b) and (c) show that the changes for the distance labels are smoother. Shown is a closer look to the image in Figure 1.

borders, i.e., a cell nuclei was morphologically eroded and another one dilated resulting in masks which only differ in single pixels. The location of the boundaries and borders change completely which makes it more difficult to train a model well. In addition, there is often only limited border information in the training images if only a few cell nuclei do really touch. The neighbor distances also provide information in the training process if nuclei are close but do not touch.

**Architecture and Training Settings** The architecture used is based on the 2D U-Net architecture [23]. However, instead of using a single decoder path, two parallel decoder paths are used which allow each decoder path to focus on features related to the desired output. The maximum pooling layers are replaced with 2D convolutional layers with stride 2 and kernel size 3. Additionally, batch normalization layers are added. The number of feature maps is doubled from 64 feature maps to a maximum of 1024 in the encoder path and halved in each decoder path correspondingly.

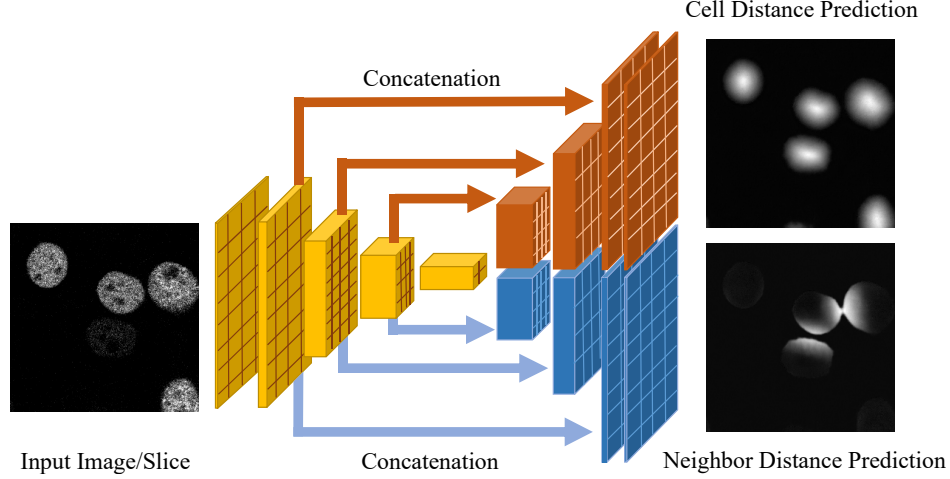


Figure 3: Convolutional neural network architecture. The input image shows a crop from the data set Fluo-N2DH-GOWT1 of the Cell Tracking Challenge [5, 22]. The image has been adapted with permission from [10].

Figure 3 shows the architecture. The rectified linear unit activation function is used within the network and a linear activation for the output layers. Models are trained for a maximum of 250 epochs with a batch size of 8 using the Adam optimizer [24] with a starting learning rate of  $8 \times 10^{-4}$ . After 12 epochs without validation loss improvement, the learning rate is multiplied with 0.25 till a minimum learning rate of  $6 \times 10^{-5}$  is reached. To learn the cell distance transformation and the cell neighbor distance transformation, PyTorch’s SmoothL1Loss is used and both losses are added. During training flipping, scaling, rotation, contrast changing, blurring and noise adding augmentations are applied. The best model was selected manually out of three trained models. However, the models’ predictions did not show large differences.

**Training Data Set** The assembled training data set consists of the provided Cell Tracking Challenge training data [5, 22], publicly available data, i.e., images from the synthetic CBIA HL60 cell line data set<sup>2</sup> [25] and drosophila images from the BBBC data set BBBC038<sup>3</sup>[3], and some generated semi-synthetic benchmarks for embryomics (data set SBDE4 in [26])<sup>4</sup>. Since some of the Cell Tracking Challenge gold truth data show only some annotated cells, and the silver truth data are not error free in any case, only selected 2D training data and slices of the 3D data are used. The final training data sets consists of 997 crops of size  $256 \times 256$  px which includes 200 crops used for validation. A more detailed description of the data set can be found on the homepage of the Cell Tracking Challenge when the results are published (team KIT-Sch-GE).

**Inference** For inference, each frame of the time series is minimum-maximum normalized independently into the range  $[-1, 1]$ . For 3D data the whole volume is normalized. For the 3D dataset Fluo-N3DL-TRIC, contrast limited adaptive histogram equalization [28] is applied to each slice. Model inputs are zero-padded if necessary. The images of the data set Fluo-C3DH-H157 are downsampled to half of the original size since very large objects tend to be oversegmented. 2D data are processed frame-by-frame. 3D data are processed slice-wise ( $xy$ -slices) and frame-by-frame.

**Post-Processing** Figure 4 shows the main steps of the post-processing. The cell distance and neighbor distance predictions are smoothed slightly (2D/3D Gaussian smoothing for 2D/3D data). Then, the region to flood with a marker-based watershed is extracted out of the smoothed cell distance prediction using simple thresholding. To get the seeds (or markers), the smoothed neighbor distance prediction taken to the power of  $a \in \{1, 2, 3, 4\}$  (depending on cell size and the neighbor distance decline) is subtracted from the cell prediction and the result is thresholded. Seeds with an area smaller than 2 are removed. The parameters for the processed Cell Tracking Challenge data sets can be found on the homepage of the Cell Tracking Challenge when the results are published (team KIT-Sch-GE). For some data sets, artifacts are removed or seeds closed using a 2D/3D morphological closing operation. Due to RAM restrictions, only

<sup>2</sup><https://cbia.fi.muni.cz/datasets/>

<sup>3</sup><https://data.broadinstitute.org/bbbc/BBBC038/>

<sup>4</sup>[27] extends this benchmark data set

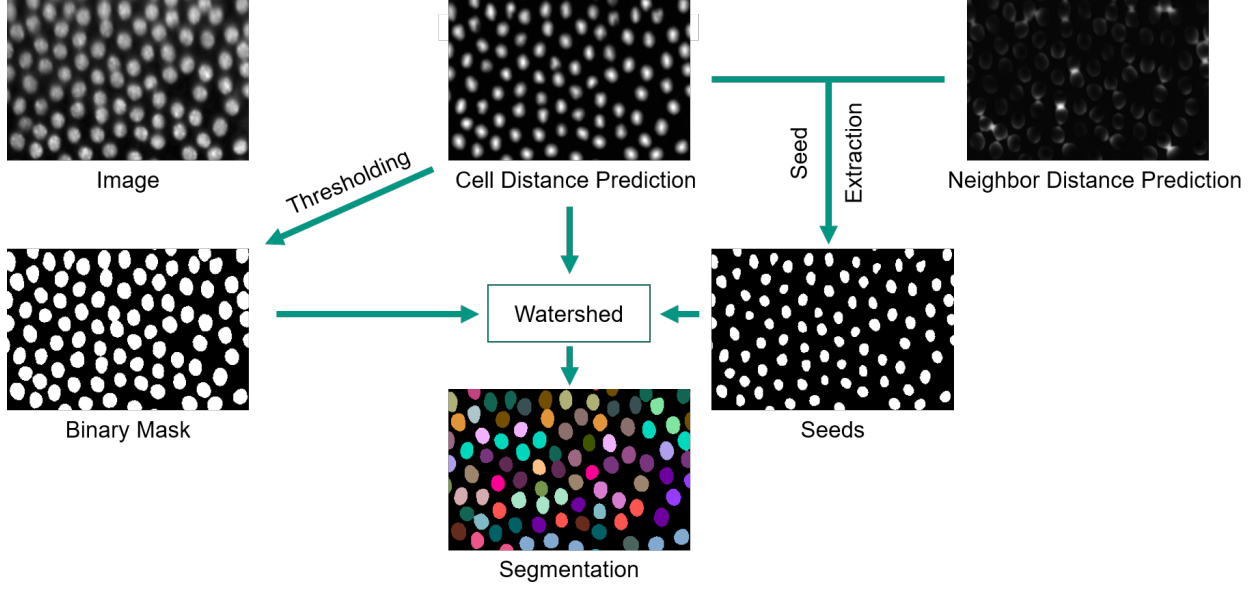


Figure 4: Overview of the main segmentation post-processing steps. The image shows a 2D crop from the data set Fluo-N3DL-TRIC of the Cell Tracking Challenge [5, 22].

each second slice of the Fluo-N3DL-TRIF data set is processed and the volume additionally split into two parts with overlap. The final Fluo-N3DL-TRIF predictions are upsampled using a nearest neighbor interpolation. For the data set Fluo-N3DL-CE, merged cell nuclei (in  $z$ -direction) are split when their volume is bigger than  $\frac{4}{3}$  times the mean object volume at that time point. Therefore, the seed extraction threshold is increased till multiple seeds are found.

## 2.2 Tracking

**Initialization** For object tracking the time steps are traversed forwards. First, for each segmented object at time step  $t_0$ , a track is initialized. For data sets with tracking seeds (Fluo-N3DL-TRIF, Fluo-N3DL-TRIC, Fluo-N3DL-DRO), tracks are initialized for segmented objects including a tracking seed. It is assumed that the object movement between successive frames is small. Therefore, for each track a ROI (region of interest) is defined as a search space for the same object in the next frame. The ROI size is fixed to - 150x150 on 2D data sets, 60x60x60 for Fluo-N3DL-TRIF, Fluo-N3DL-TRIC, Fluo-N3DL-DRO, and 100x100x100 on all other 3D data sets. The initial center of each ROI is set to the median position of each segmented object at  $t_0$ .

**Tracking Step** The tracking step is split into a movement estimation followed by a graph-based matching. To estimate the object movement between successive frames, a displacement between successive images  $I_t$  and  $I_{t+1}$  is computed. The displacement is estimated by calculating a cross correlation between the ROI at  $I_t$  and  $I_{t+1}$  for each track. Based on the estimated displacements, the ROIs at time step  $t + 1$  are adapted.

Next, for each active track at time steps  $\{t - \Delta t, \dots, t\}$ , a set of potential matching candidates is selected based on its ROI at time step  $t + 1$ . A track is considered active if: it has no successors and the last time step an object has been assigned to it,  $t_{last}$ , is at most  $t - t_{last} \leq \Delta t$  steps apart from  $t$ .

Active tracks and the potential matching candidates are matched by using an adapted version of the by Padfield et al. proposed graph-based coupled minimum-cost flow algorithm [29]. The matching algorithm minimizes the overall matching cost between active tracks and potential matching candidates subject to a set of constraints modeling flow, appearance/disappearance of objects, and splitting/merging of objects.

Figure 5 provides an overview of the adapted graph structure. The by Padfield et al. [29] proposed algorithm has been adapted as follows : No merging events are considered, as the original algorithm models only merging of two objects per time step. The appearance costs of objects are set to 0, as spurious tracks will be filtered out by the subsequent post-processing. Furthermore, this appeared to be advantageous in scenarios with the objective to track only a few

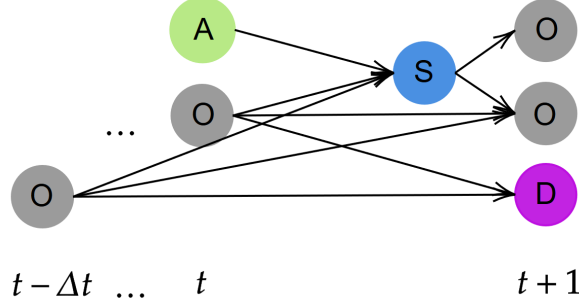


Figure 5: Graph-based matching algorithm adapted from Padfield et al. [29]. Gray nodes are segmented objects (O). The green node models the appearance of objects (A), whereas the pink node models disappearance of objects (D). Cell divisions are modeled by the blue node (S). All active tracks from time steps  $\{t - \Delta t, \dots, t\}$  are added to the graph and matched with the segmented objects at time step  $t + 1$ . Some edges are added to the graph exemplarily.

selected objects. The matching cost  $c_{s,n}$  between track  $s$  and potential matching candidate  $n$  is adapted to:

$$c_{s,n} = \|\hat{p}_{t+1}^s - p_{t+1}^n\|_2,$$

where  $\hat{p}_{t+1}^s$  is the estimated position of track  $s$  at time  $t + 1$  and  $p_{t+1}^n$  the position of the potential matching candidate. The estimated position  $\hat{p}_{t+1}^s$  is given by :

$$\hat{p}_{t+1}^s = p_t^s + d^s,$$

where  $d^s$  is the estimated displacement of the ROI of track  $s$  between time step  $t$  and  $t + 1$ .  $p_t^s$  is the median position of the tracked object at time step  $t$ . The costs of split events are computed based on size and position of the tracked object and its potential successor candidates. As each active track can only be linked to segmented objects overlapping with its ROI, the number of edges in the graph is reduced. Moreover, all active tracks are added to the graph and not only objects between successive time steps. This procedure helps to account for single segmentation errors as tracks can be re-linked. For tracks with missing segmentation masks, the position is linearly interpolated between  $t + 1$  and  $t_{last}$  and segmentation masks are added at the missing time steps. For data sets with the goal to track all objects, each non-matched object at time step  $t + 1$  is initialized as a new track.

**Post-Processing** In the post-processing step trajectories of length one without any predecessor and successors are removed. Furthermore, frames without any tracked object are replaced by the tracking result of the temporally closest frame.

### 2.3 Implementation Details

Segmentation and tracking are implemented in Python. As deep learning framework PyTorch is used. For Linux-based systems, deployable executables compiled using pyinstaller can be downloaded from the Cell Tracking Challenge homepage. We recommend to have at least 32 GiB RAM and 24 GiB VRAM to be able to process also the large Cell Tracking Challenge data sets. For the other data sets, 16 GiB RAM and 12 GiB VRAM work as well.

## 3 Author Contributions

Tim Scherr designed and implemented the segmentation procedure. Katharina Löffler designed and implemented the tracking procedure. Moritz Böhlend and Tim Scherr developed the idea of the neighbor distance transforms. Tim Scherr and Katharina Löffler wrote the paper. Ralf Mikut supervised the project. All authors discussed the results and commented on the paper.

## 4 Acknowledgments

This work has been supported by the Helmholtz Association in the program BioInterfaces in Technology and Medicine (BIFTM), and the Helmholtz Information & Data Science School for Health (HIDSS4Health).



## References

- [1] A. Y. Kobitski *et al.*, “An Ensemble-Averaged, Cell Density-Based Digital Model of Zebrafish Embryo Development Derived from Light-Sheet Microscopy Data with Single-Cell Resolution,” *Scientific Reports*, vol. 5, pp. 1–10, 2015.
- [2] K. Khairy and P. J. Keller, “Reconstructing Embryonic Development,” *Genesis*, vol. 49, pp. 488–513, 2011.
- [3] J. C. Caicedo *et al.*, “Nucleus Segmentation Across Imaging Experiments: The 2018 Data Science Bowl,” *Nature Methods*, vol. 16, pp. 1247–1253, 2019.
- [4] B. Schott *et al.*, “EmbryoMiner: A New Framework for Interactive Knowledge Discovery in Large-Scale Cell Tracking Data of Developing Embryos,” *PLOS Computational Biology*, vol. 14, pp. 1–18, 2018.
- [5] V. Ulman *et al.*, “An Objective Comparison of Cell-Tracking Algorithms,” *Nature Methods*, vol. 14, pp. 1141–1152, 2017.
- [6] J. Stegmaier *et al.*, “Fast Segmentation of Stained Nuclei in Terabyte-Scale, Time Resolved 3D Microscopy Image Stacks,” *PLOS ONE*, vol. 9, pp. 1–11, 2014.
- [7] J. C. Caicedo *et al.*, “Evaluation of Deep Learning Strategies for Nucleus Segmentation in Fluorescence Images,” *Cytometry A*, 2019.
- [8] T. Scherr *et al.*, “Best Practices in Deep Learning-Based Segmentation of Microscopy Images,” in *Proceedings 28. Workshop Computational Intelligence, Dortmund*, pp. 175–195, KIT Scientific Publishing, 2018.
- [9] F. A. G. Peña *et al.*, “J Regularization Improves Imbalanced Multiclass Segmentation,” 2019, arXiv: 1910.09783.
- [10] X. Li *et al.*, “Dual U-Net for the Segmentation of Overlapping Glioma Nuclei,” *IEEE Access*, vol. 7, pp. 84040–84052, 2019.
- [11] J. Li, Z. Hu and S. Yang, “Accurate Nuclear Segmentation with Center Vector Encoding,” in *Information Processing in Medical Imaging*, pp. 394–404, Springer International Publishing, 2019.
- [12] S. Graham *et al.*, “Hover-Net: Simultaneous Segmentation and Classification of Nuclei in Multi-Tissue Histology Images,” *Medical Image Analysis*, vol. 58, p. 101563, 2019.
- [13] G. Ciaparrone *et al.*, “Deep Learning in Video Multi-Object Tracking: A Survey,” *Neurocomputing*, vol. 381, pp. 61 – 88, 2020.
- [14] R. Yao *et al.*, “Video Object Segmentation and Tracking: A Survey,” 2019, arXiv: 1904.09172.
- [15] C. Payer *et al.*, “Segmenting and Tracking Cell Instances with Cosine Embeddings and Recurrent Hourglass Networks,” *Medical Image Analysis*, vol. 57, pp. 106–119, 2019.
- [16] T. He *et al.*, “Cell Tracking Using Deep Neural Networks with Multi-Task Learning,” *Image and Vision Computing*, vol. 60, pp. 142–153, 2017.
- [17] K. E. G. Magnusson *et al.*, “Global Linking of Cell Tracks Using the Viterbi Algorithm,” *IEEE Transactions on Medical Imaging*, vol. 34, no. 4, pp. 911–929, 2015.
- [18] P. Dendorfer *et al.*, “CVPR19 Tracking and Detection Challenge: How Crowded Can It Get?,” 2019, arXiv: 1906.04567.
- [19] J. Pont-Tuset *et al.*, “The 2017 DAVIS Challenge on Video Object Segmentation,” 2018, arXiv: 1704.00675.
- [20] N. Xu *et al.*, “YouTube-VOS: A Large-Scale Video Object Segmentation Benchmark,” 2018, arXiv: 1904.09172.
- [21] T. Sixta and B. Flach, “Multiple Object Segmentation and Tracking by Bayes Risk Minimization,” in *Medical Image Computing and Computer-Assisted Intervention – MICCAI 2016* (S. Ourselin *et al.*, eds.), vol. 9901, pp. 607–615, Springer International Publishing, 2016.
- [22] M. Maška *et al.*, “A Benchmark for Comparison of Cell Tracking Algorithms,” *Bioinformatics*, vol. 30, no. 11, pp. 1609–1617, 2014.
- [23] O. Ronneberger, P. Fischer and T. Brox, “U-Net: Convolutional Networks for Biomedical Image Segmentation,” in *Medical Image Computing and Computer-Assisted Intervention – MICCAI 2015*, pp. 234–241, Springer International Publishing, 2015.
- [24] D. Kingma and J. Ba, “Adam: A Method for Stochastic Optimization,” in *International Conference on Learning Representations (ICLR)*, 2014, arXiv: 1412.6980v9.
- [25] D. Svoboda, M. Kozubek and S. Stejskal, “Generation of Digital Phantoms of Cell Nuclei and Simulation of Image Formation in 3D Image Cytometry,” *Cytometry Part A*, vol. 75A, no. 6, pp. 494–509, 2009.

- [26] J. Stegmaier, *New Methods to Improve Large-Scale Microscopy Image Analysis with Prior Knowledge and Uncertainty*. PhD thesis, Karlsruher Institut für Technologie (KIT), 2017.
- [27] J. Stegmaier *et al.*, “Generating Semi-Synthetic Validation Benchmarks for Embryomics,” in *2016 IEEE 13th International Symposium on Biomedical Imaging (ISBI)*, pp. 684–688, 2016.
- [28] S. Pizer *et al.*, “Adaptive Histogram Equalization and its Variations,” *Computer Vision, Graphics, and Image Processing*, vol. 39, no. 3, pp. 355 – 368, 1987.
- [29] D. Padfield, J. Rittscher and B. Roysam, “Coupled Minimum-Cost Flow Cell Tracking for High-Throughput Quantitative Analysis,” *Medical Image Analysis*, vol. 15, no. 4, pp. 650 – 668, 2011. Special section on IPMI 2009.